Journal of the Korean Astronomical Society
52: 41 ∼ 47, 2019 April

https://doi.org/10.5303/JKAS.2019.52.2.41
pISSN: 1225-4614 · eISSN: 2288-890X
http://jkas.kas.org

Measuring Timing Properties of PSR B0540–69

Minjun Kim and Hongjun An

Department of Astronomy and Space Science, Chungbuk National University, Cheongju 28644, Korea;
iehatro@chungbuk.ac.kr, hjan@chungbuk.ac.kr

Received July 10, 2019; accepted February 20, 2019

Abstract: We report on the timing properties of the 'Crab twin' pulsar PSR B0540−69 measured with X-ray data taken with the *Swift* telescope over a period of 1100 days. The braking index of the pulsar was estimated to be $n = 0.03 \pm 0.013$ in a previous study performed in 2015 with 500-day *Swift* data. This small value of n is unusual for pulsars, and a comparison with an old estimate of $n \approx 2.1$ for the same target determined ∼10 years earlier suggests a dramatic change in the braking index. To confirm the small value and therefore the large change of n, we used 1100-day *Swift* observations including the data used in the earlier determination of $n = 0.03$. In this study we find that the braking index of PSR B0540−69 is $n = 0.163 \pm 0.001$, somewhat larger than 0.03. Since the measured value of n is still much smaller than 2.1, we can confirm the dramatic change in the braking index for this pulsar.

Key words: pulsars: general — pulsars: individual (PSR B0540−69) — X-rays: stars

1. Introduction

Neutron stars are the left-over cores of massive stars after a supernova explosion. They are composed of extremely dense matter and have very strong magnetic fields ($\sim 10^{12}$ G). They are usually detected as pulsating (rotating) sources in the radio to γ-ray band (Ostriker & Gunn 1969). Their spin frequency slowly decreases and timing properties in this spinning-down process can be characterized by measuring the spin frequency ν and its time derivatives $\dot{\nu}$ and $\ddot{\nu}$ which are combined to derive the braking index $n = \ddot{\nu}\nu/\dot{\nu}^2$ (Manchester et al. 1985).

Measuring the braking index for pulsars is difficult because the measurement requires an estimation of the second derivative which is very small in general. In addition, the rotation of neutron stars is known to be irregular due to 'glitches', sudden changes in the spin-down rate, and due to 'timing noise', long-term non-periodic modulations. Thus pulsar timing properties can be characterized only by observing the pulsars for a long time. Up to now braking indices have been measured for only about 10 of the about 2600 detected pulsars (Table 1), with typical values below 3 (Lyne et al. 2015).

The braking index of a pulsar can be used to understand its energy-loss mechanisms. For ideal magnetic dipole radiation, the braking index is expected to be around 3 (Lyne et al. 2015), but it can differ due to other energy loss mechanisms (e.g., wind and gravitational wave) or to changes in the mechanical properties. Values $n \sim 1$ can occur if the energy loss of a pulsar is dominated by the wind, or $n \sim 5$ if gravitational-wave radiation is dominant (Kou & Tong 2015; de Araujo et al. 2016). Effects due to changes in the mechanical properties on n are very complex. Several of these effects may operate at the same time, and by measuring n, one can infer which effect is dominant. The evolution of a pulsar can be studied because the changes on n can imply any effect of the aforementioned mechanisms.

Until now, a wide range of values for n has been measured. Although the measured braking indices for various pulsars can be between −1.2 (PSR J0537−6910, perhaps contaminated by frequent glitches; Antonopoulou et al. 2018) or 0.9 (PSR J1734−3333; Espinoza et al. 2011) and 3.15 (PSR J1640−4631; Archibald et al. 2016), most cases are only within $2 \leq n \leq 3$ (Lyne et al. 2015). Furthermore, n has been observed to change in some pulsars; the braking index of PSR J1119−6127 changed from 2.91 to 2.684 when a glitch occurred (Antonopoulou et al. 2015) and that of PSR J1846−0258 changed from 2.65 to 2.19 after an outburst (Archibald et al. 2015). While it is not yet clearly understood how various pulsars have so different values of n and how they change, some theories have been developed: accretion from a hypothetical fall-back disk (Menou et al. 2001), super-fluid decoupling (Antonopoulou et al. 2018), magnetic-field evolution (Gourgouliatos & Cumming 2015; Blandford & Romani 1988), and an effective change in the moment of inertia (Sedrakian & Cordes 1998). Because there are not many pulsars with a measured braking index, understanding the value and its change on a firm theoretical ground is still lacking. It is therefore crucial to measure n and its changes for a larger number of sources to identify extreme cases and to constrain the models.

PSR B0540−69 is a young and bright 50-ms pulsar in the Large Magellanic Cloud (Seward et al. 1984). The pulsar is surrounded by a pulsar wind nebula (PWN, $R_{\rm pwn} \approx 4''$; Kaaret et al. 2001) which has a morphology (torus and jet; Campana et al. 2008; Mignani et al. 2012) similar to that of the Crab nebula (Mori

Corresponding author: H. An

Table 1
List of pulsars with a measured braking index

Pulsar	ν (Hz)	$\dot{\nu}$ (10^{-10}s^{-2})	$\nu/2\dot{\nu}$ (kyr)	n	Reference
J0534+2200	29.946923	−3.77535	1.26	2.342(1)	Lyne et al. (2015)
J0537−6910	62	−1.992	4.93	−1.22(4)	Antonopoulou et al. (2018)
J0835−4510	11.200	−0.15375	11.3	1.7(2)	Espinoza et al. (2017)
J1119−6127	2.4512027814	−0.2415507	1.6	2.91(5)∼2.684(2)	Antonopoulou et al. (2015)
J1208−6238	2.26968010518	−0.16842733	2.67	2.598(1)	Clark et al. (2016)
J1513−5908	6.611515243850	−0.6694371307	1.56	2.832(3)	Livingstone et al. (2011)
J1640−4631	4.843410287	−0.2280830	3.4	3.15(3)	Archibald et al. (2016)
J1734−3333	0.855182765	−0.0166702	8.13	0.9(2)	Espinoza et al. (2011)
J1833−1034	16.15935711336	−0.52751130	4.85	1.857(1)	Roy et al. (2012)
J1846−0258	3.0621185502	−0.6664350	0.73	2.65(1)∼2.16(1)	Archibald et al. (2015)

et al. 2004; Madsen et al. 2015). The rotation properties are well measured up to the second derivative, with a characteristic age $\tau_c = \nu/2\dot{\nu}$ of $\sim$ 1700 years and a braking index of $n \approx 2.1$ (e.g., Livingstone et al. 2005). The most interesting property of this pulsar is a large change in the braking index which was measured to be $n = 2.123 \pm 0.012$ between 1999 and 2011 with *RXTE* in $2 - 60$ keV band (Ferdman et al. 2015) but which a recent study reported to be $n = 0.031 \pm 0.013$ using 500 days of *Swift* observations taken between 2015 and 2016 (Marshall et al. 2016). Such a large change and small value of n have not been seen in any other pulsar. The braking index of $n \approx 2.1$ before 2010 seems to be reliable because several works have obtained similar values ($n \approx 2.1$) by independently analyzing long (>10 years) *RXTE* and/or *BeppoSAX* ($2 - 30$ keV) observations (Cusumano et al. 2003; Livingstone et al. 2005; Ferdman et al. 2015; Zhang et al. 2001). However, the value $n = 0.03$ derived from 500-day *Swift* data in Marshall et al. (2016) has not been carefully examined. Thus, a careful reinvestigation is needed.

In this work, we reanalyzed the 500-day *Swift* data used in Marshall et al. (2016) to confirm their timing solution. We then added more recent additional 600 days of *Swift* data to extend the baseline and to refine the braking index measurement. We describe the observations in Section 2 and present the timing analysis and the results in Section 3. We then discuss and conclude in Section 4.

2. OBSERVATIONS AND DATA REDUCTION

We used X-ray data of PSR B0540−69 observed by the *Swift* X-ray telescope (Gehrels et al. 2004) between 2015 Feb. 17 and 2018 Feb. 11. Note that the baseline of the observations we used is about twice that used in Marshall et al. (2016). In this period, 62 *Swift* observations with a typical exposure of ∼2 ks were performed using the window timing mode (with a time resolution of 1.7 ms) to facilitate measurements of the short 50-ms period of the pulsar. We processed the observational data using the standard *Swift* pipeline incorporated in `HEASOFT 6.20` along with the latest `CALDB` calibration files. We selected events using a $R = 20''$ circular region centered at the source position in the 0.7–7 keV band. The photon arrival times were corrected to the solar system barycenter using the source position $\alpha = 05^h40^m11.202^s$ and $\delta = -69°19'54.17''$ (Mignani et al. 2010) and the JPL DE200 ephemeris. Because of the short 94-min orbital period of the *Swift* satellite, long observations suffer from Earth occultations which cause gaps in the data. To remove occultation artifacts (e.g., beats), we split an observation into continuous segments when the observation is longer than the *Swift* orbital period. After pre-calibration and selection, there were 208–1369 photons per segment.

3. TIMING ANALYSIS

Young pulsars like PSR B0540−69 tend to be more active (e.g., showing more glitches and timing noise); therefore, their timing properties seem to be more irregular (e.g., Dib & Kaspi 2014). Indeed, Livingstone et al. (2005) and Ferdman et al. (2015) found some glitches and relatively large timing noise. The latter is a particular concern in the results of Marshall et al. (2016) because they did not find any timing noise. Non-detection of timing noise in their work implies that the pulsar timing noise was significantly smaller in 2015 than in 2010. Marshall et al. (2016) noted that there could be small timing noise but it would not change their results significantly. Alternatively, it is also possible that there was significant timing noise in 2015–2016, but the 500-day observations could not distinguish between the real timing behavior (timing solution) and the long-term timing noise because the baseline (∼500 days) was too short.[1] In this case, their timing solution would have been biased due to the noise. The characteristic time scale of the timing noise in PSR B0540−69 was ∼700 days (e.g., Ferdman et al. 2015), and hence, if this trend persisted, timing noise can be characterized only by using data with a > 700-day baseline. Thus, the timing behavior of PSR B0540−69 described by the *Swift* observations needs to be re-investigated carefully.

There are several ways to determine a pulsar timing solution. Here we considered two methods: direct period measurements for the individual time series and

[1] Usually "timing solution" refers to the real timing behavior and the long-term noise taken together. Here, however, we separate them for clarity.

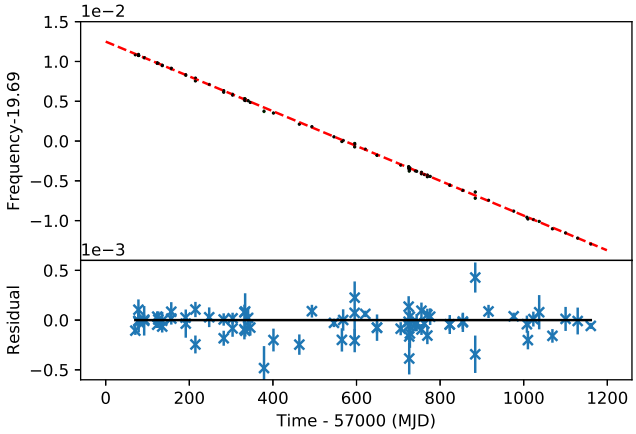

Figure 1. Results of the direct frequency measurement using the Z_1^2-test. *Top*: Frequencies measured for each continuous data segment (black data points) and a linear fit (red solid line) to measure the frequency derivative. *Bottom*: Residuals left after subtracting the best-fit linear function.

phase connection. The former uses the Z_1^2-test (de Jager et al. 1989) to measure the periodicity in individual observations. This is a robust method for period detection that is insensitive to minor irregularities but also to the timing properties. Phase connection is more sensitive to timing noise because it uses both the periodicity and the pulse shape, but requires the observations to be inspected within specific time intervals. The observation data that we use satisfied the time-interval requirement for the phase connection method; therefore, we used this more sensitive technique which enabled us to measure $\ddot{\nu}$ and the timing noise. The aforementioned two methods may result in different solutions when the baseline is long and the pulsar exhibits a timing anomaly during the observations (e.g., An et al. 2013).

3.1. Direct Frequency Measurements

We first used the more robust but less sensitive method, the Z_1^2-test (Buccheri et al. 1983) for a sanity check. This test basically computes the Z_1^2 statistic value for a light curve folded into assumed periods. The Z_1^2 value is large if there is periodicity at some frequency, so one can find the best ν that maximizes the Z_1^2 value by scanning ν near the known value ($\nu \approx 19.696$ Hz for PSR B0540−69). Uncertainties for ν measurements were obtained by running simulations. We did this for each data segment and show the best frequencies that we determined in Figure 1. It is clear from the figure that the frequency changes with time; hence, we measured the first derivative ($\dot{\nu}$) by fitting the frequency trend with a linear function. The fit was acceptable with $\chi^2_{\rm min}/dof = 46.3/71$, and the best-fit frequency and the derivative are $\nu = 19.69633(1)$ Hz and $\dot{\nu} = -2.533(3) \times 10^{-10}$ s^{-2} at the epoch of MJD 57281.24147641701, respectively. 1-σ uncertainties are estimated by scanning ν and $\dot{\nu}$ to find a range for the parameters in which χ^2 is less than $\chi^2_{\rm min} + 2.3$. We also used fitting with a quadratic function to measure

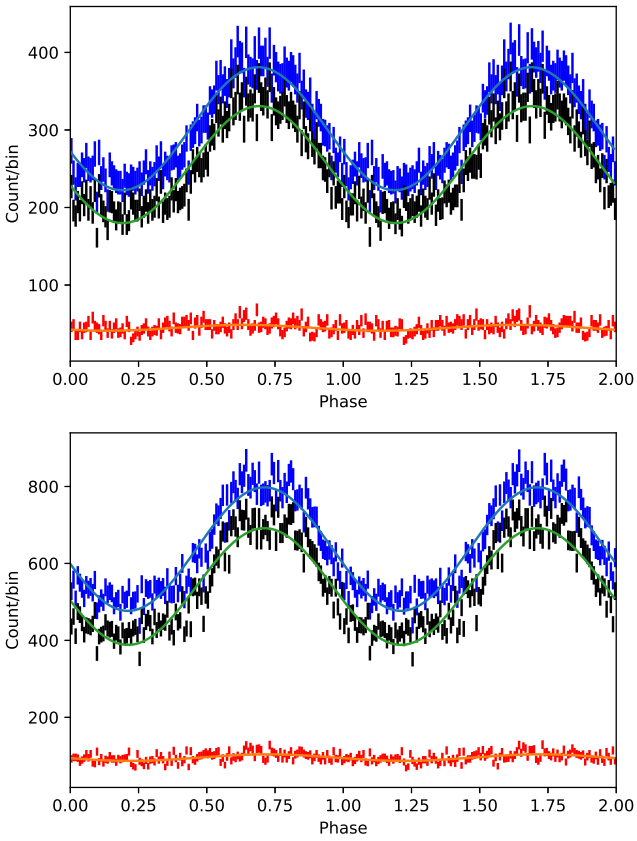

Figure 2. 0.5–7-keV pulse profiles of PSR B0540−69. *Top*: The pulse profiles in the first ∼500 days of data produced with the known timing solution of Marshall et al. (2016). *Bottom*: The pulse profile made with the 1100-day data and the refined solution. Blue and black points are pulse profiles of the source before and after background subtraction, respectively. Best-fit sine functions are shown as smooth lines, the background profile is shown in red. We used 128 bins for the profiles and show two cycles for clarity. The profiles for the 500-day and 1100-day data appear similar, with pulsed fractions of 0.295(6) and 0.280(4).

the second derivative ($\ddot{\nu}$) but the uncertainty for the quadratic term is large, so we only derived a 90% upper limit of $\ddot{\nu} < \ddot{\nu}_{\rm best} + 1.28\Delta\ddot{\nu} = 2.9 \times 10^{-20}$ s^{-3}, assuming a normal distribution. Because we cannot measure $\ddot{\nu}$ with this method, we tried a more sensitive method described below.

3.2. Phase Semi-Coherent Method

We applied the phase-connection method (phase semi-coherent analysis) to measure the second derivative of the period. The phase semi-coherent method (e.g., see Livingstone et al. 2005) starts from an existing timing solution for the first data set (a part of the whole data) to be analyzed and gradually improves the solution by adding more data. With the first data set and the timing solution for the data, a rotation phase for each detected photon is computed using $\phi(t) = \phi_0 + \nu t + \frac{1}{2}\dot{\nu}t^2 + \frac{1}{6}\ddot{\nu}t^3$, where $\phi(t)$ is the rotation phase of the photon detected at time t; ϕ_0 is the reference

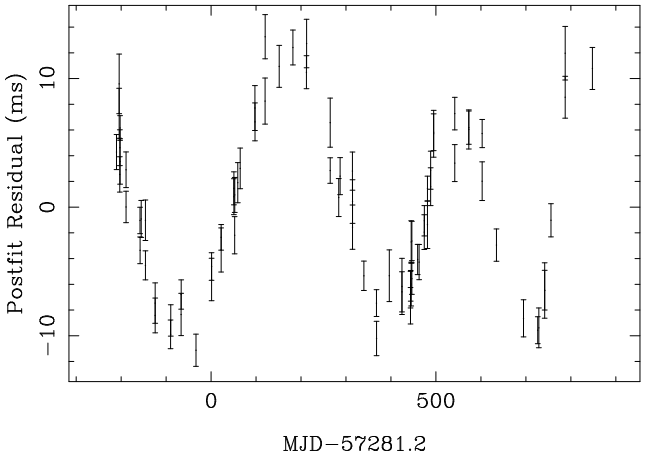

Figure 3. Timing residuals after fitting out the cubic trend (timing solution) from the phase-shift measurements of the 1100-day data.

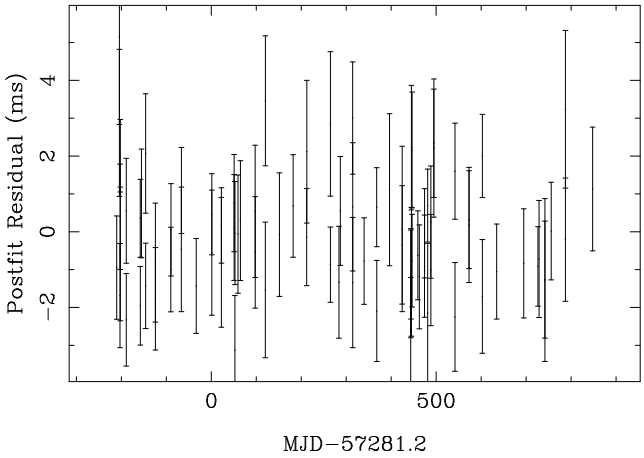

Figure 4. Timing residuals obtained in TEMPO2 after whitening the timing noise.

phase, and ν and its derivatives are the timing solution. An initial pulse profile is generated by constructing the phase histogram (pulse profile, see Figure 2 bottom). Using the initial timing solution, we construct the pulse profile for the next observation and compare with the previous profile. Although the two pulse profiles can be compared directly, it is better to use a continuous function to represent the pulse profiles to reduce the effects of statistical fluctuations. Thus, we model the profiles with a sine function (Figure 2) and check if the profiles align (no relative shift, i.e., phase-connect). If the phase shift of the new profile with respect to the previous one is less than 1 cycle ($\Delta\phi < 1$), we keep including the next data. Note that we were not seriously concerned about the fit between the profile and the sinusoidal function because we compare the relative shift only. As we keep doing this, the phase shift with respect to the initial profile may get larger (slow drift with time) and eventually become larger than 1 and thus, we are not able to phase-connect the new profile to the initial one if the initial timing solution is not perfect. If this occurs, we update the timing solution by varying ν, $\dot{\nu}$, and $\ddot{\nu}$ to phase-connect all the data up to the point just before the disconnection. We repeat this procedure until the last observation. In this process, it may not be possible to phase-connect all the data perfectly (i.e., without relative shift) with only three timing parameters ν, $\dot{\nu}$, and $\ddot{\nu}$, and there may be small ($\ll 1$) relative phase shifts between observations which cannot be modeled with our polynomial of degree 3. These residual phase shifts are usually attributed to timing noise.

Before proceeding to analyze the 1100-day data, we confirmed the previous results (see Table 2) by actually fitting the 500-days data with the same data used to infer $n = 0.03$ (25 *Swift* observations made between MJDs 57070 and 57546; Marshall et al. 2016). We find $\nu = 19.696323386(2)$ s^{-1}, $\dot{\nu} = 2.528649(1) \times 10^{-10}$ s^{-2}, and $\ddot{\nu} = 0.16(3) \times 10^{-21}$ s^{-3}, yielding $n = 0.05(1)$. These are consistent with the previous solution within statistical uncertainties. We found no clear timing noise in the data as Marshall et al. (2016) already noted. Thus, we used these 500-day data and the timing solution of Marshall et al. (2016) as our starting points and gradually added new data taken from MJDs 57546 to 58161 in the analysis, extending the baseline to 1100 days. Although the initial solution was valid for the first 500-day data, we found that the phase shifts get larger with time and that the profiles do not phase-connect to the initial one after ∼30 additional days. We therefore refined the timing solution to phase-connect the later profiles and repeated this to the last data set to construct a long-term 1100-day timing solution. After fitting the rotational behavior (timing solution up to the cubic term), there still appear to be relative phase shifts between the pulse profiles measured at different epochs (Figure 3). These timing residuals are the timing noise. We also show the pulse profile constructed with the whole 1100-day data in the bottom panel of Figure 2 which is similar to the initial one (Figure 2 upper panel). The new timing solution is presented in Table 2.

We note that the timing noise pattern in Figure 3 is similar to that measured by Livingstone et al. (2005) and Ferdman et al. (2015) using >10 y data. Additionally, notice that even in the first ∼500 days, there is a residual long-term trend (timing noise) which was not seen when using the previous timing solution.

3.3. Timing Noise

Physical origin and evolution of timing noise are not yet well understood and are therefore unpredictable. Only by using a long baseline can timing noise (high-order polynomials) be distinguished from the timing solution (low-order polynomials). However, the concern is that there can be some mixing between the solution and the noise. Thus, the timing solution may change a little if we model the timing noise with high-order polynomials or sine functions and fit the data (e.g., Figure 3) to include the noise model. A standard way to model

Table 2
Several timing solutions for PSR B0540−69 obtained in previous works as well as this work

	Marshall	This Work (after whitening)	This Work (before whitening)
Observation date (MJD)	57070∼57546	57070∼58068	
Epoch (MJD)	57281.24	57281.24	
ν (Hz)	19.6963233901(22)	19.696323365(1)	19.696323365(2)
$\dot{\nu}$ (10^{-10}s^{-2})	−2.5286507(15)	−2.528664(1)	−2.528664(2)
$\ddot{\nu}$ (10^{-21}s^{-3})	0.104(41)	0.531(4)	0.531(8)
Braking index (n)	0.031(13)	0.163(1)	0.164(1)

and fit the timing noise is to use the power spectrum of the timing residual ('whitening'). This method can be applied to the residuals (Figure 3) with the TEMPO2 package (Hobbs et al. 2006).[2] We performed whitening using TEMPO2, and the whitened residuals are shown in Figure 4. The changes in the timing solution due to the whitening are insignificant. As a crosscheck, we fitted the phase residual data with a timing noise model, polynomials or sinusoidal functions and find that n changes from 0.163 (before whitening) to 0.164 (after whitening). These two are statistically consistent. We found that the change in the timing solution is very small in this case as well (see Table 2).

4. DISCUSSION

We measured the timing properties of PSR B0540−69 using the *Swift* data covering 1100 days. The timing solution obtained with the more robust Z_1^2 test is consistent with that measured with the phase-coherent method. The values measured for measured ν, $\dot{\nu}$, and $\ddot{\nu}$ with the phase-coherent method imply a braking index of $n = 0.163 \pm 0.001$. We further attempted to model or whiten the timing noise and found that the timing solution is not sensitive to the timing noise models.

The solution we obtained for PSR B0540−69 is different from the previous ones (see Table 2; Livingstone et al. 2005; Ferdman et al. 2015; Marshall et al. 2016). The discrepancy with those in Livingstone et al. (2005) or Ferdman et al. (2015) can be easily understood because our measurements were done far later in time than theirs; PSR B0540−69 is a young and active pulsar, and thus, the timing properties might have changed due to glitches or a spin-state transition (significant change in the rotational properties). Indeed Marshall et al. (2015) suggested a spin-state transition in MJD 55900 after two glitches in MJD 51348 and MJD 52925; hence, solutions measured before (e.g., Livingstone et al. 2005; Ferdman et al. 2015) and after (this work and Marshall et al. 2016) can differ. The discrepancy with that of Marshall et al. (2016) is small but still statistically significant. We attribute the discrepancy to the timing noise. Perhaps, their results may be biased by undetermined timing noise. By properly isolating and accounting for the timing noise, we were able to determine the timing solution more accurately.

[2] http://www.atnf.csiro.au/research/pulsar/tempo2/

Based on our new solution, we can estimate the bias due to the timing noise in the previous result. As shown in Figure 3, the timing noise in the first ∼500 days seems to follow a cubic trend with an amplitude of ∼10 ms ($\phi_{\rm max} \approx 0.2$). We therefore modeled the residuals with a cubic function: $\phi(t) = at^3 + bt^2 + ct + d$, where we reset the zero of the time t to be at MJD 57546.08, the last data point in the 500-days time span. We find $a = -3.82 \times 10^{-22}$ s^{-3}, b $= 1.73 \times 10^{-15}$ s^{-2}, and $c = 2.22 \times 10^{-8}$ s^{-1} in the fit. These values can be compared with $\phi(t)$ in section 3.2, resulting in $\ddot{\nu}_{\rm bias} = 6a = -2.3 \times 10^{-21}$ s^{-3}, $\dot{\nu}_{\rm bias} = 2b = 3.5 \times 10^{-15}$ s^{-2}, and $\nu_{\rm bias} = c = 2.22 \times 10^{-8}$ s^{-1}, which are sufficient for explaining the discrepancy. Hence, we argue that indeed the previous solution is biased due to the timing noise. This concern, however, was already noted in Marshall et al. (2016); the authors argued that the effects of the timing noise would not be large. Our quantitative analysis suggests that the impact of the timing noise on the solution and n is statistically significant but is small in absolute terms, as they argued.

As noted above, the most intriguing features of PSR B0540−69 are the extremely small value and the large change of n over time. We arrive at the same conclusion with our study performed with a more accurate timing solution; we confirmed the main conclusion of Marshall et al. (2016). Although such a small value of n and large change (likely accompanied with the state change; Marshall et al. 2015) are not yet well understood, it is suggested that evolution of the magnetic field in the neutron star (Gourgouliatos & Cumming 2015), changes of mechanical properties of the pulsar (Sedrakian & Cordes 1998), and/or a putative accretion disk (e.g., accretion rate; Menou et al. 2001) may result in a small value of n and the change. We found that $n = 0.163$ was larger than the previous one ($n = 0.031$). While this difference could be due to timing noise, it may also imply some changes in the pulsar or in the putative disk.

Timing changes often occur contemporaneously with a radiative change but in PSR B0540−69 no significant evidence for a radiative change was found (Marshall et al. 2015). However, PSR B0540−69 is in a crowded region of the sky and is surrounded by a PWN (Kaaret et al. 2001). The 16″ angular resolution of *Swift* is not enough to resolve the pulsar from the 4′ nebula or the nearby sources. Furthermore, the *Swift* observations

are all taken in timing mode without 2D images. Thus, unchanging (constant in time) contamination from the nearby sources and the PWN may dominate the flux, making accurate measurements of small changes in the pulsar flux hard. Future *Chandra* observations (0.5″ angular resolution) for spatially resolved spectroscopy (e.g., An et al. 2014) may be useful to measure a change in the flux of the pulsar and/or the nebula.

We finally note that a further timing analysis with longer (>500 days) *Swift* data has been performed by Marshall et al. (2018). They reported that the braking index n of PSR B0540−69 is still near 0, but details of the timing solution are not avaliable. It would be interesting to check if they detected the timing noise and if their timing solution agrees with ours. This can be done in the near future.

ACKNOWLEDGMENTS

This research was supported by the Basic Science Research Program through the National Research Foundation of Korea (NRF) funded by the Ministry of Science, ICT & Future Planning (NRF-2017R1C1B2004566).

REFERENCES

An, H., Kaspi, V. M., Archibald, R., & Cumming, A. 2013, Spectral and Timing Properties of the Magnetar CXOU J164710.2-455216, ApJ, 763, 82

An, H., Madsen, K. K., Reynolds, S. P., et al. 2014, High-Energy X-Ray Imaging of the Pulsar Wind Nebula MSH 15-52: Constraints on Particle Acceleration and Transport, ApJ, 793, 90

Antonopoulou, D., Weltevrede, P., Espinoza, C. M., et al. 2015, The Unusual Glitch Recoveries of the High-Magnetic-Field Pulsar J1119−6127, MNRAS, 447, 3924

Antonopoulou, D., Espinoza, C. M., Kuiper, L., et al. 2018, Pulsar Spin-Down: the Glitch-Dominated Rotation of PSR J0537−6910, MNRAS, 473, 1644

Archibald, R. F., Kaspi, V. M., Beardmore, A. P., et al. 2015, On the Braking Index of the Unusual High-B Rotation-Powered Pulsar PSR J1846−0258, ApJ, 810, 67

Archibald, R. F., Gotthelf, E. V., Ferdman, R. D., et al. 2016, A High Braking Index for a Pulsar, ApJ, 819, L16

Blandford, R. D., & Romani, R. W. 1988, On the Interpretation of Pulsar Braking Indices, MNRAS, 234, 57

Buccheri, R., Bennett, K., Bignami, G, F., et al. 1983, Search for Pulsed Gamma-Ray Emission From Radio Pulsars in the COS-B Data, A&A, 128, 245

Campana, R., Mineo, T., de Rosa, A., et al. 2008, X-Ray Observations of the Large Magellanic Cloud Pulsar PSR B0540−69 and Its Pulsar Wind Nebula, MNRAS, 389, 691

Clark, C. J., Pletsch, H. J., Wu, J., et al. 2016, The Braking Index of a Radio-Quiet Gamma-Ray Pulsar, ApJL, 832, L15

Cusumano, G., Massaro, E., & Mineo, T. 2003, Timing Noise, Glitches and the Braking Index of PSR B0540−69, A&A, 402, 647

de Araujo, J. C. N., Coelho, J. G., & Costa, C. A. 2016. Gravitational Waves from Pulsars with Measured Braking Index, Eur. Phys. J. C, 76, 481

de Jager, O. C., Raubenheimer, B. C., & Swanepoel, J. W. H. 1989, A Powerful Test for Weak Periodic Signals with Unknown Light Curve Shape in Sparse Data, A&A, 221, 180

Dib, R., & Kaspi, V. M., 2014, 16 yr of RXTE Monitoring of Five Anomalous X-Ray Pulsars, ApJ, 784, 37

Espinoza, C. M., Lyne, A. G., Kramer, M., et al. 2011, The Braking Index of PSR J1734−3333 and the Magnetar Population, ApJ, 741, 1

Espinoza, C. M., Lyne, A. G., & Stappers, B. W., 2017, New Long-Term Braking Index Measurements for Glitching Pulsars Using a Glitch-Template Method, MNRAS, 466, 147

Ferdman, R. D., Archibald, R. F., & Kaspi, V. M. 2015, Long-Term Timing and Emission Behavior of the Young Crab-Like Pulsar PSR B0540−69, ApJ, 812, 95

Gehrels, N., Chincarini, G., Giommi, P., et al. 2004, The Swift Gamma-Ray Burst Mission, ApJ, 611, 1005

Gourgouliatos, K. N., & Cumming, A. 2015, Hall Drift and the Braking Indices of Young Pulsars, MNRAS, 446, 1121

Hobbs, G. B., Edwards, R. T., & Manchester, R. N. 2006, TEMPO2, A New Pulsar-Timing Package – I. An Overview, MNRAS, 369, 655

Kaaret, P., Marshall, H. L., Aldcroft, T. L., et al. 2001, Chandra Observations of the Young Pulsar PSR B0540-69, ApJ, 546, 1159

Kou, F. F., & Tong, H. 2015, Rotational Evolution of the Crab Pulsar in the Wind Braking Model, MNRAS, 450, 1990

Livingstone, M. A., Kaspi, V. M., & Gavriil, F. P. 2005, Long-Term Phase-Coherent X-Ray Timing of PSR B0540−69, ApJ, 633, 1095

Livingstone, M. A., Ng, C. Y., Kaspi, V. M., et al. 2011, Post-Outburst Observations of the Magnetically Active Pulsar J1846-0258. A New Braking Index, Increased Timing Noise, and Radiative Recovery, ApJ, 730, 66

Livingstone, M. A., & Kaspi, V. M. 2011, Long-Term X-Ray Monitoring of the Young Pulsar PSR B1509-58, ApJ, 742, 31

Lyne, A. G., Jordan, C. A., Graham-Smith, F., et al., 2015, 45 Years of Rotation of the Crab Pulsar, MNRAS, 446, 857

Madsen, K. K., Reynolds, S., Harrison, F., et al. 2015, Broadband X-Ray Imaging and Spectroscopy of the Crab Nebula and Pulsar with NuSTAR, ApJ, 801, 66

Manchester, R. N., Durdin, J. M., & Newton, L. M. 1985, A Second Measurement of a Pulsar Braking Index, Nature, 313, 374

Marshall, F. E., Guillemot, L., Harding, A. K., et al. 2015, Discovery of a Spin-Down State Change in the LMC Pulsar B0540-69, ApJ, 807, L27

Marshall, F. E., Guillemot, L., Harding, A. K., et al. 2016, A New, Low Braking Index for the LMC Pulsar B0540−69, ApJ, 827, L39

Marshall, F. E., Guillemot, L., Harding, A. K., et al. 2018, On-Going Monitoring of the LMC Pulsar B0540-69, American Astronomical Society Meeting Abstracts #231, 231, #243.05

Menou, K., Perna, R., & Hernquist, L. 2001, Stability and Evolution of Supernova Fallback Disks, ApJ, 559, 1032

Mignani, R. P., Sartori, A., de Luca, A., et al. 2010, HST/WFPC2 Observations of the LMC Pulsar PSRB0540−69, A&A, 515, A110

Mignani, R. P., De Luca, A., Hummel, W., et al. 2012, The Near-Infrared Detection of PSR B0540−69 and Its Nebula, A&A, 544, A100

Mori, K., Burrows, D. N., Hester, J. J., et al. 2004, Spatial Variation of the X-Ray Spectrum of the Crab Nebula, ApJ, 609, 186

Ostriker, J. P., & Gunn, J. E. 1969, On the Nature of Pulsars. I. Theory, ApJ, 157, 1395

Roy, J., Gupta, Y., & Lewandowski, W. 2012, Observations of Four Glitches in the Young Pulsar J1833−1034 and Study of Its Glitch Activity, MNRAS, 424, 2213

Sedrakian, A., & Cordes, J. M. 1998, Spin Evolution of Pulsars with Weakly Coupled Superfluid Interiors, ApJ, 502, 378

Seward, F. D., Harnden. Jr, F. R., & Helfand, D. J. 1984, Discovery of a 50 Millisecond Pulsar in the Large Magellanic Cloud, ApJ, 287, L19

Zhang, W., Marshall, F. E., Gotthelf, E. V., et al. 2001, A Phase-Connected Braking Index Measurement for the Large Magellanic Cloud Pulsar PSR B0540−69, ApJ, 554, L177